SUPPLEMENTARY INFORMATION

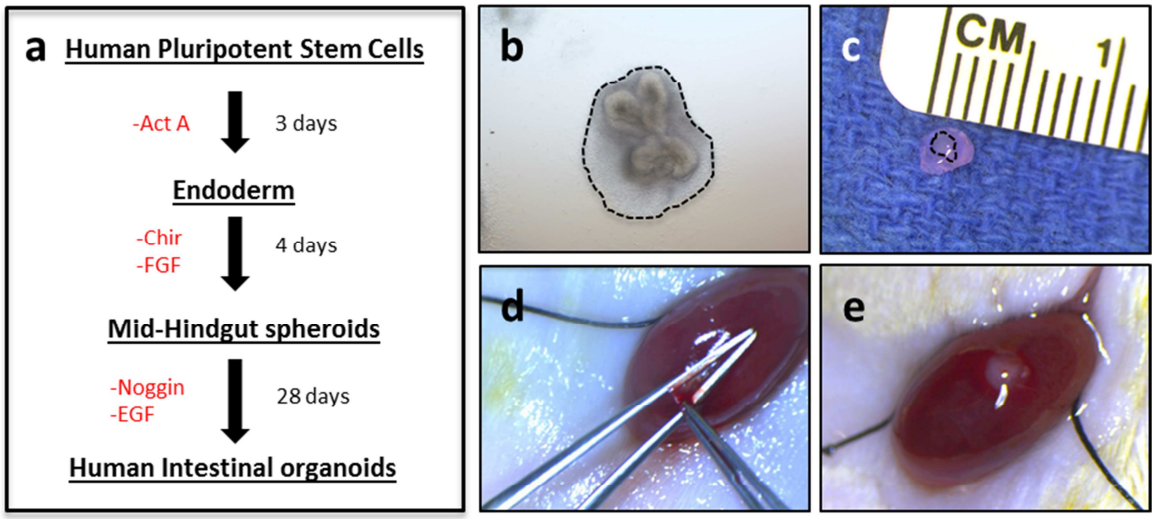

f

Total # Transplant	Surviving Mice	Visible Engraftment	Cartilage %	Intestinal Tissue (Pure)	Efficiency of engraftment (Pure)
145	144/145 (99.3%)	139	5/139 (3.6%)	134	134/145 (92.4%)

Supplementary Figure 1: Timeline/Schematic of HIO production, Size and Engraftment Efficiency. (a) Schematic representing directed differentiation of HIOs from hPSCs over a period of 35 days. **(b)** Picture of HIO prior to transplant revealing central epithelium and surrounding supporting mesenchyme (outlined). **(c)** Relative size of one HIO (outlined) embedded in type I collagen prior to transplant. **(d)** Creation of pocket under kidney capsule using fine forceps. **(e)** Picture of transplanted HIO under kidney capsule. **(f)** Table showing efficiency of engraftments at 6 week time point after transplantation.

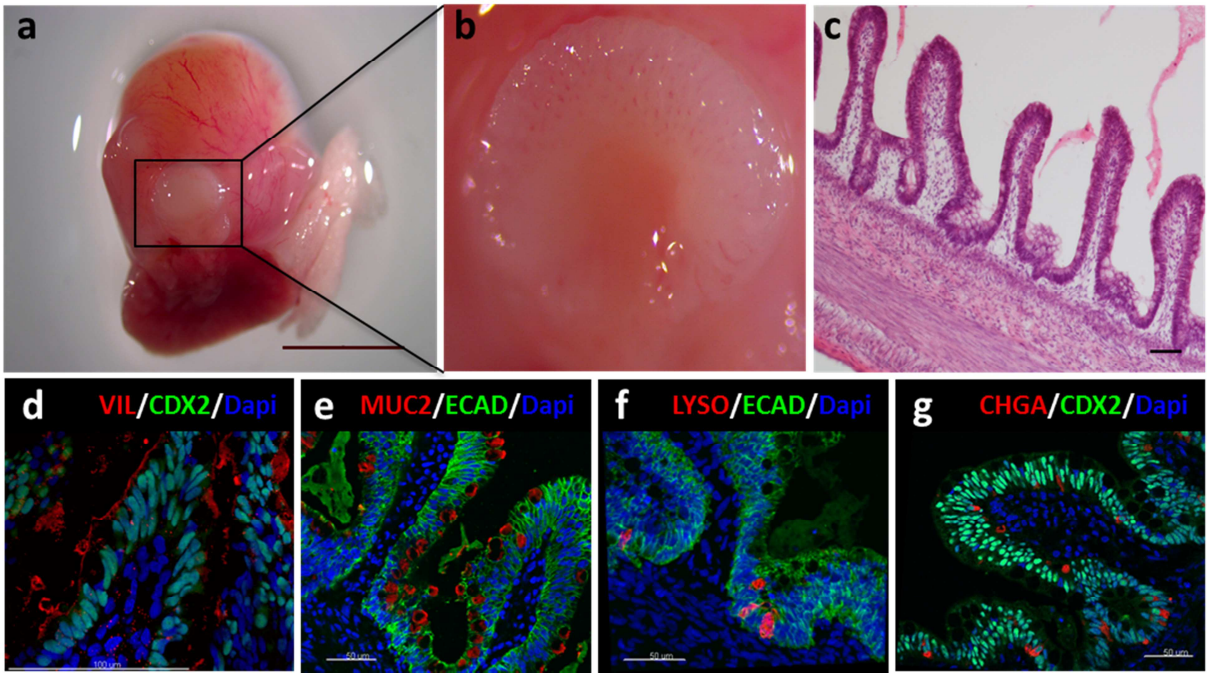

Supplementary Figure 2: HIOs from induced pluripotent stem cells engraft to form mature human intestinal tissue *in vivo.* **(a)** Engraftment 6 weeks after transplant using HIO derived from induced pluripotent stem cells. **(b)** Magnified image of engraftment revealing luminal surface of engraftment with villi and central capillaries. **(c)** Magnified H&E of epithelium within engraftment (Scale bar 100 µm). Crypt-villus domains were present as well as appropriate layers of sub-epithelium including lamina propria, muscularis mucosa, submucosa, and laminated outer smooth muscle layers. **(d-g)** All 4 intestinal lineages were present in engraftments including enterocytes (Villin- VIL) (Scale bar 100 µm) **(d)**, Goblet cells (Mucin-MUC2) **(e)**, Paneth cells (Lysozyme- LYSO) **(f)**, and enteroendocrine cells (Chromogranin A-CHGA) **(g)**. E-cadherin (ECAD) or CDX2 were used for additional epithelial staining. (All scale bars 50 um except where specified).

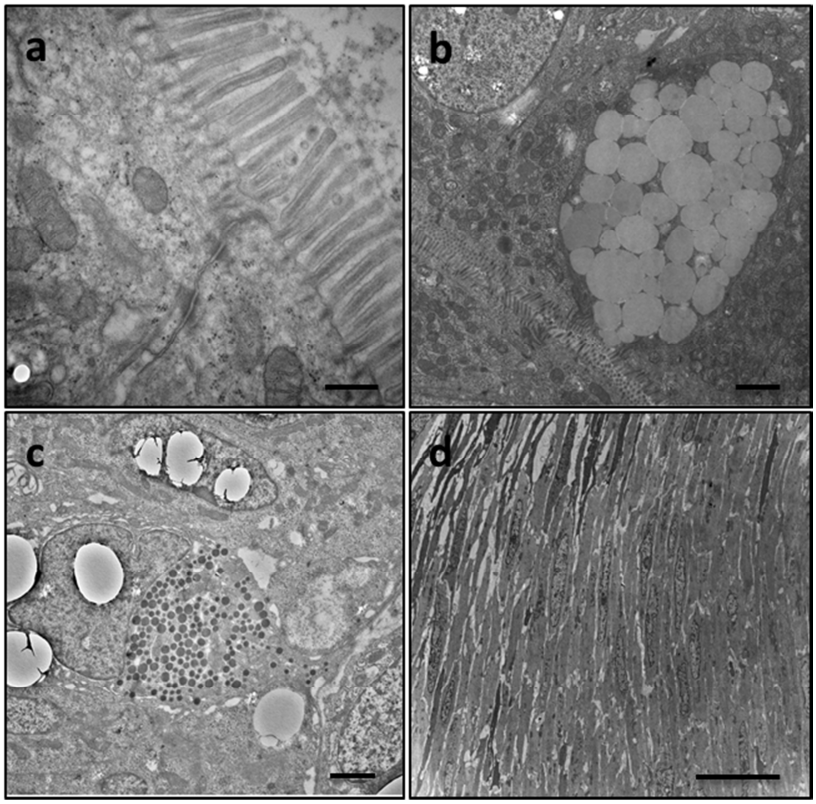

Supplementary Figure 3: Transmission Electron Microscopy (TEM) of engrafted tissue at 6 weeks. **(a)** TEM image of brush border microvilli on the surface of intestinal epithelium. Tight and adherens junctions can also be seen in this image near the apical surface (scale bar 500 nm). **(b)** TEM image of goblet cell with secretory granules (white) containing mucin (scale bar 2 μm). **(c)** TEM image of enteroendocrine cell with secretory granules (dark) ready for release on basolateral aspect of cell (scale bar 2 μm). **(d)** TEM image of smooth muscle within engraftment with parallel orientation of smooth muscle fibers (scale bar 10 μm).

Nature Medicine: doi:10.1038/nm.3737

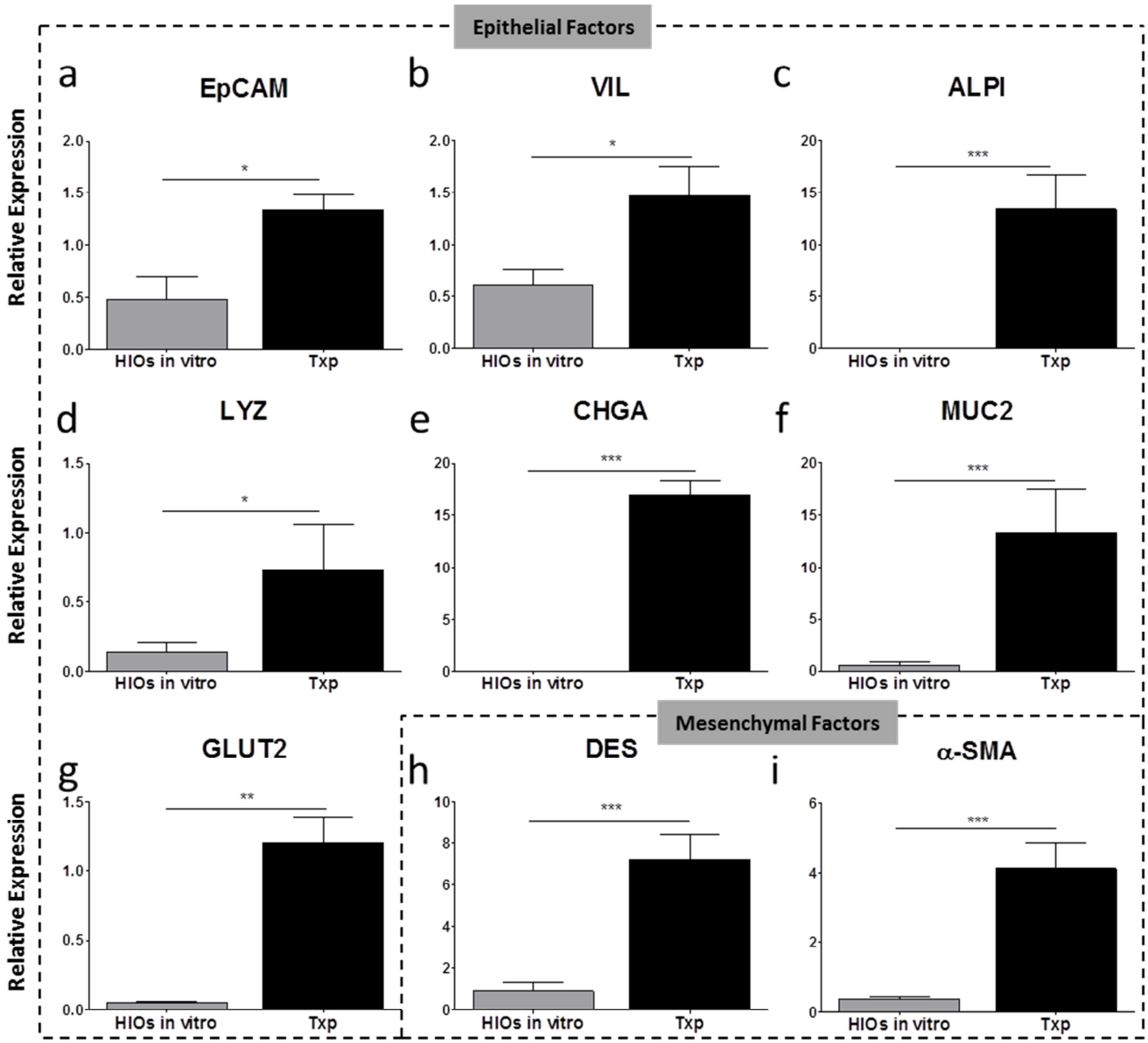

Supplementary Figure 4: Additional epithelial and mesenchymal markers of maturity in transplanted HIOs vs HIOs *in vitro*. (a-g) Comparison of relative gene expression of epithelial markers including EpCAM **(a)**, Villin (VIL) **(b)**, Alkaline phosphatase (ALPI) **(c)**, Lysozyme (LYZ) **(d)**, Chromogranin A (CHGA) **(e)**, Mucin (MUC2) **(f)**, and Glucose transporter 2 (GLUT2) **(g)**. **(h-i)** Relative expression of smooth muscle markers Desmin (DES) **(h)** and smooth muscle actin (α-SMA) **(i)**. Values in graphs represent Mean ± s.e.m. ns, not significant. *, p <0.05; **, p<0.01; ***, p<0.001; HIOs in vitro: n=4; Transplants (Txp): n=8.

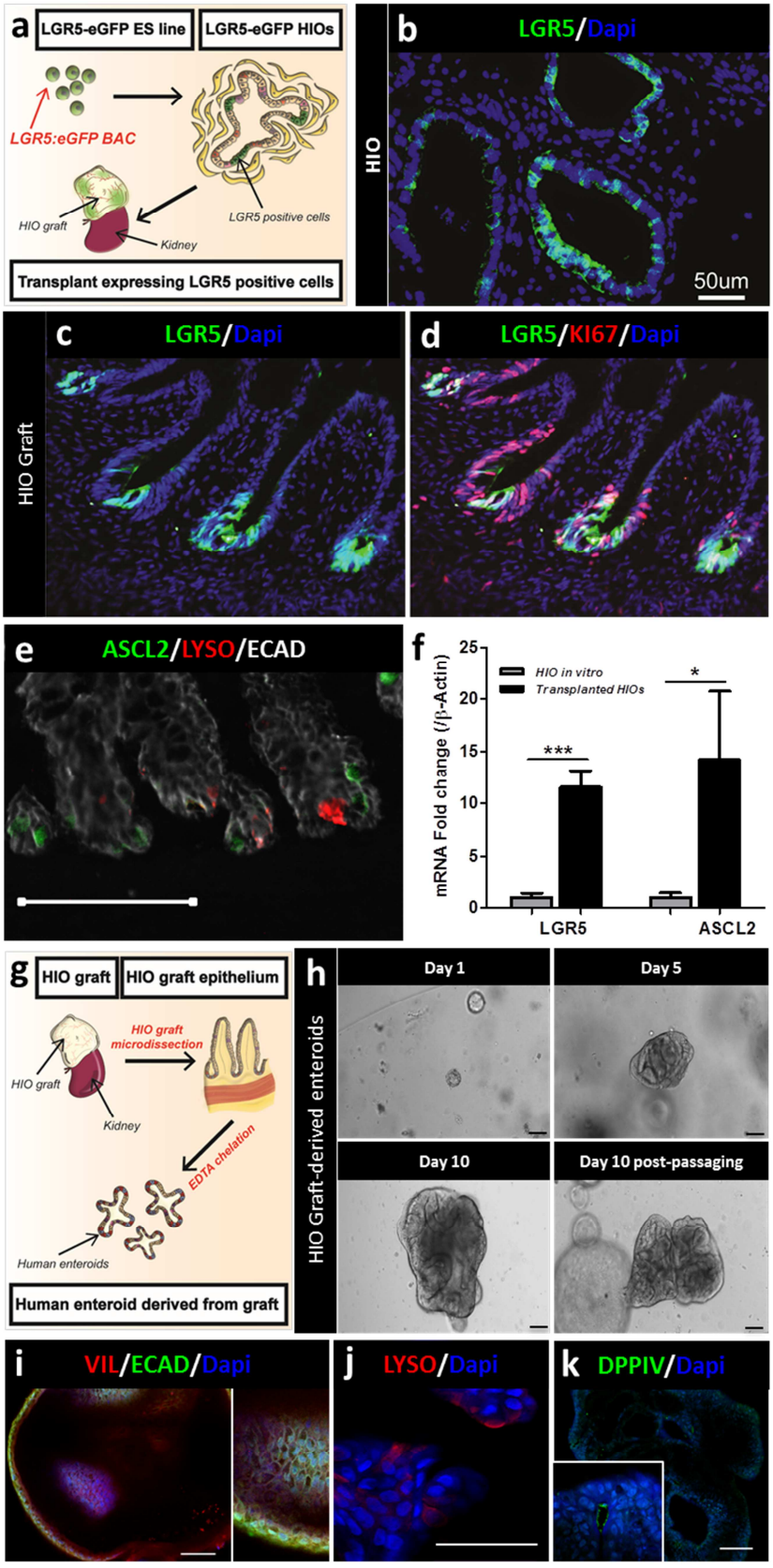

Nature Medicine: doi:10.1038/nm.3737

Supplementary Figure 5: Engrafted tissue displayed a mature epithelium maintained by intestinal stem cells. (a-d) An LGR5R5:eGFP BAC reporter ES line has been established and was used to generate HIOs expressing LGR5-eGFP cells **(a).** LGR5-eGFP cells (green) were seen within an HIO *in vitro* scattered throughout the epithelium **(b)** and are localized in proliferative crypt base cells (colocalization with KI67), as expected in engrafted human intestinal tissue **(c-d)**. **(e)** Immunofluorescence staining of stem cell marker ASCL2 (green) localized within the crypt bases of the engraftment. **(f)** Graph demonstrated relative fold changes of LGR5 and ASCL2 within HIOs *in vitro* prior to transplant and in engraftments. **(g)** Enteroids were generated from the engrafted epithelium to demonstrate the stemness of the tissue. **(h)** Panel shows Engraftment-derived epithelial enteroids following initial plating at days 1, 5, and 10 and after passaging. **(i-k)**. Immunofluorescence staining revealed the presence of epithelial cells with Villin (VIL) and E-cadherin (ECAD) **(i)** as well as the presence of Paneth cells (Lysozyme - LYSO) **(j)** and brush border enzyme (Dipeptidyl peptidase 4 - DPPIV) **(k)** (All scale bars 50 µm).

Nature Medicine: doi:10.1038/nm.3737

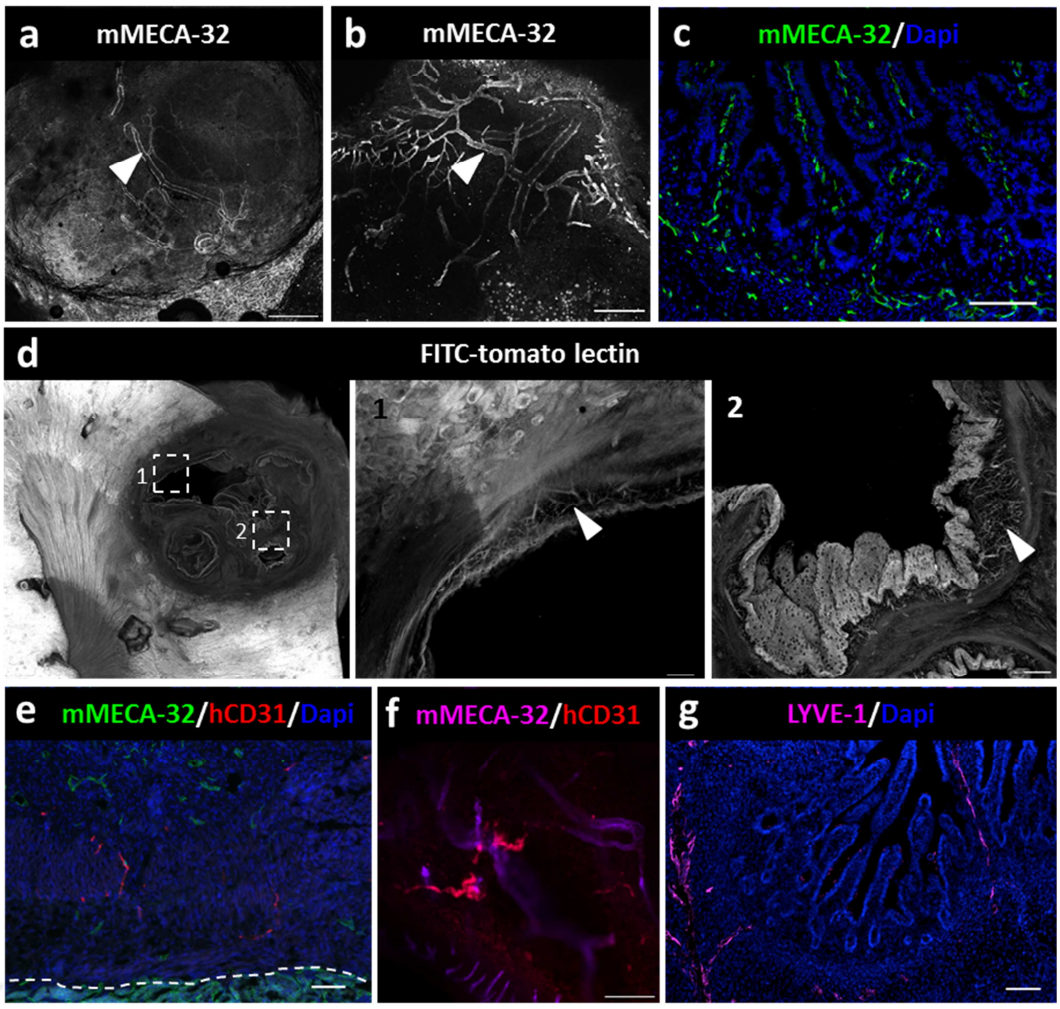

Supplementary Figure 6: Engrafted intestinal tissue received its blood supply from the ingrowth of murine vasculature. **(a)** A panendothelial antibody specific to mouse (mMECA-32) is used to reveal murine vasculature just below the surface of an engraftment **(b)** as well as within the interior of an engraftment (white arrowheads; Scale bars 50 µm). **(c)** Magnified immunofluorescence image of mMECA-32 stained endothelium (green) comprising the vasculature within each villi as well as the capillary plexus just beneath the epithelium within the engraftment. **(d)** Whole mount staining of engraftment within the kidney following FITC-labelled tomato lectin injections via mouse tail vein. Outlined areas 1 and 2 correspond with following images revealing functional fluorescent murine vasculature within the engraftments (Scale bars 50 µm). **(e)** Immunofluorescence image revealing murine-specific (mMECA-32) and human specific (hCD31) staining of endothelium within an engraftment. **(f)** Confocal imaging on whole mount engraftments did not showed connections between the murine and human vasculature. **(g)** A murine specific marker of lymphatic vessels (LYVE-1) demonstrated ingrowth of lymphatic vessels from the murine host. (All scale bars 100 µm except where specified).

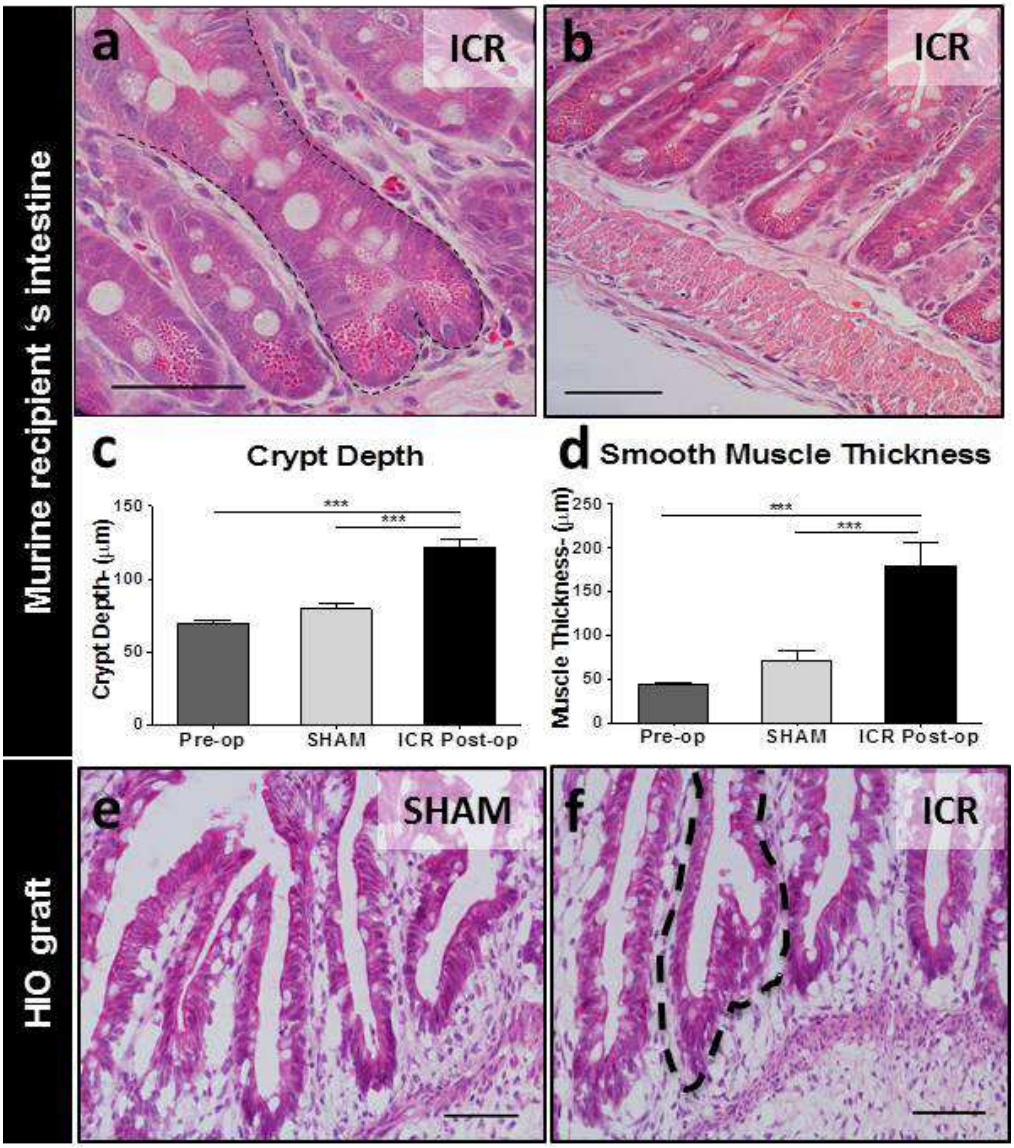

Supplementary Figure 7: NSG Mice also undergo intestinal adaptation following surgical resection as well as the HIO graft. **(a)** Magnified image of crypt fission (outlined) in murine small intestine following resection. (Scale bar 50 µm). **(b)** Increased thickness of smooth muscle layer (tunica muscularis) in postoperative ICR tissue (Scale bar 50 µm). **(c)** Comparison in murine intestinal crypt depth (µm) between Pre-operative, sham, and resected (ICR) groups. **(d)** Comparison of thickness of smooth muscle layer (µm) in Pre-operative, sham, and resected (ICR) groups. **(e)** Magnified image of intestinal epithelium in HIO graft in a sham mouse (Scale bar 50 µm). **(f)** Magnified image of crypt fission (outlined) in HIO graft in an ICR mouse (Scale bar 50 µm). Values represented in graphs represent Mean ± s.e.m. ns, not significant. *, $p < 0.05$; **, $p < 0.01$; ***, $p < 0.001$; Pre-op group: n=13; sham group: n=10; ICR group: n=11.

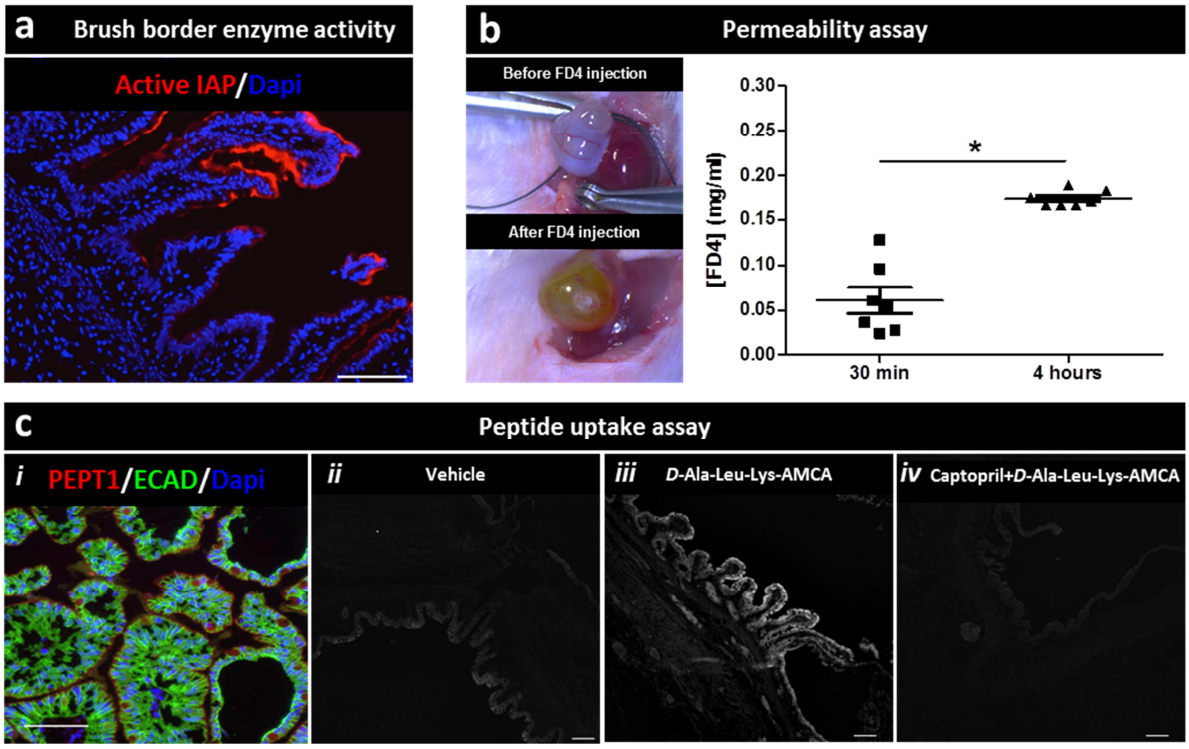

Supplementary Figure 8: Engrafted human intestinal tissue retained digestive and absorptive function. (a) Intestinal alkaline phosphatase demonstrated activity *ex vivo* (Scale bar 100 um). **(b)** FITC-Dextran (MW 4,400) injected into engraftments *in vivo* (pictures seen before and after) increased significantly in murine serum from initial timepoint of 30 minutes compared with timepoint of 4 hours within each mouse (n=7). Values represented in graph represent Mean ± s.e.m.; ns, not significant; *, p <0.05; **, p<0.01; ***, p<0.001; paired t-test. **(c)** D-Ala-Leu-Lys-AMCA peptide uptake assay revealing peptide transporter (PEPT1) staining within the epithelium of an engraftment (scale bar 100 µm) ***(i)***. Additional images showing fluorescence within the epithelium following injections of vehicle (DMEM solution), D-Ala-Leu-Lys-AMCA (DMEM + labeled peptide solution), and Captopril + D-Ala-Leu-Lys-AMCA (DMEM + labeled peptide + competitive inhibitor of transport solution) (n=3 for each group). Fluorescence was observed following injection of labeled peptide ***(iii)***, but little to no fluorescence was observed with either vehicle injection ***(ii)*** or with labeled-peptide + captopril injection ***(iv)***.

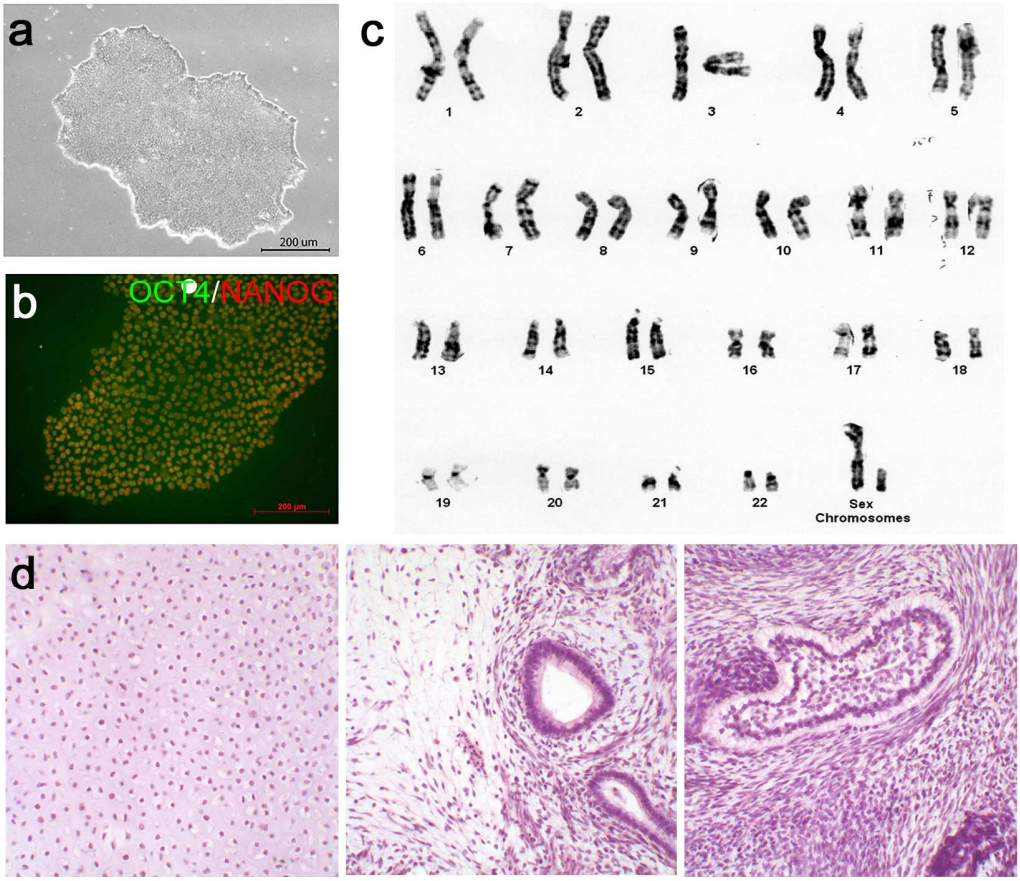

Supplementary Figure 9: Quality control assays for iPSCs. (a) Phase contrast image of iPSC colonies cultured in standard feeder free conditions. **(b)** Immunofluorescence staining of pluripotency markers Oct4 and Nanog in iPSCs. **(c)** G-banded karyotype analysis demonstrating normal (46,XY) karyotype of control iPSCs. **(d)** H&E stained sections of a teratoma derived from iPSCs showed tissue arising from the three embryonic germ layers, endoderm, ectoderm and mesoderm. Control teratomas presented stellate reticular cells surrounded by peripheral epithelium with anti-basal nuclei consistent with primitive tooth (ectoderm), ciliated columnar epithelium consistent with intestine (endoderm), and cartilage cells (mesoderm). The images are 400-fold magnification.

Table S1: List of primary and secondary antibodies used for immunostaining.

Provider	Label	Host	Reactivity	Name	Cat. Number	Dilution
Primary Ab						
Abcam		Goat	Mouse, Human	Vimentin (VIM)	ab11256	1:500
Sigma		Mouse	Human	aplhaSMA (α-SMA)	Ab8207	Prediluted
R&D		Goat	Mouse, Human	E-cadherin (Ecad)	AF648	1:500
R&D		Rat	Mouse, Human	E-cadherin (Ecad)	MAB 7481	1:500
Dako		Rabbit	Human	Lysozyme (Lyz)	A0099	1:1000
Immunostar		Rabbit	Mouse, Human	Chromogranin A (ChgA)	20085	1:500
Santa-Cruz		Rabbit	Mouse, Human	Mucin 2 (MUC2)	sc-15334	1:200
Millipore	Cy 3	Mouse	Human	Human Nuclear (HuNuc)	MAB 1281C3	1:500
Biogenex		Mouse	Human	CDX2-88 (CDX2)	AM392	1:300
Sigma		Rabbit	Human	Lactase-gycosylceramidase (LCT)	HPA007408	1:500
Novus Biologicals		Rat	Mouse	MECA-32	NB100-77668	1:500
Santa-Cruz		Goat	Mouse, Human	Gastric Inhibitory Peptide (GIP)	sc-23554	1:500
Santa-Cruz		Goat	Mouse, Human	Villin	sc-7672	1:100
R&D		Goat	Mouse, Human	DPPIV	AF954	1:500
DSHB		Mouse	Human	Sucrase-Isomaltase (SIM)	HBB2/614/88	1:500
eBioscience	eF 660	Rat	Mouse	Lyve-1	50-0443	1:500
Santa-Cruz		Rabbit	Mouse, Human,Rat	Peptide Transporter 1 (Pept1)	Sc-20653	1:500
Millipore	FITC	Mouse	Human	Achaete Scute homolog 2 (ASCL2)	FCMAB285F	1:20
Pierce-Thermo		Mouse	Human	CD31/PECAM-1	MA5-15336	1:500
Secondary Ab						
Invitrogen	AF488	Donkey	Goat	Goat IgG	A11055	1:500
Invitrogen	AF555	Goat	Rabbit	Rabbit IgG	A21428	1:500
Invitrogen	AF488	Donkey	Rat	Rat IgG	A21208	1:500
Invitrogen	AF488	Donkey	Rabbit	Rabbit IgG	A21206	1:500
Invitrogen	AF546	Donkey	Mouse	Mouse IgG	A10036	1:500
Invitrogen	AF647	Donkey	Goat	Goat IgG	A21447	1:500
Invitrogen	AF555	Goat	Mouse	Mouse IgG2a	A21137	1:500
Invitrogen	AF546	Donkey	Rabbit	Rabbit IgG	A10040	1:500
Invitrogen	AF555	Donkey	Goat	Goat IgG	A21432	1:500
Invitrogen	AF488	Rabbit	Goat	Goat IgG	A11078	1:500
Invitrogen	AF 488	Donkey	Mouse	Mouse IgG	A21202	1:500

Invitrogen	AF 568	Donkey	Mouse	Mouse IgG	A10037	1:500
Jackson-Imm.	Cy5	Goat	Rat	Rat IgG	112-175-143	1:500

Table S2: List of Human Taqman® Probes used for RT-PCR.

Human TaqMan® Probes						
Gene	**Gene Name**	**Gene ID**	**TaqMAN #**	**Accession #**	**Amplicon Lengh (bp)**	**Marker type**
ALPI	Alkaline Phosphatase, intestinal	248	Hs00357579_g1	NM_001631.3	56	Enterocyte
CHGA	Chromogranin A	1113	Hs00900375_m1	NM_001275.3	88	Enteroendocrine cell
LYZ	Lysozyme	4069	Hs00426232_m1	NM_000239.2	67	Paneth cell
MUC2	Mucin 2	4583	Hs03005103_g1	NM_002457.2	53	Goblet cell
EpCAM	Epithelial Cell Adhesion Molecule	4072	Hs00901885_m1	NM_002354.2	95	Epithelium/Enterocyte
VIM	Vimentin	7431	Hs00185584_m1	NM_003380.3	73	Mesenchyme/Fibroblast
ACTA2	alpha-2, Smooth muscle actin	59	Hs00426835_g1	NM_001141945.1	105	Smooth Muscle
DES	Desmin	1674	Hs00157258_m1	NM_001927.3	83	Fibroblasts/Smooth Muscle
SI	Sucrase-Isomaltase (alpha-glucosidase)	6467	Hs00356112_m1	NM_001041.3	64	Enterocyte
VILL	Villin-like	50853	Hs00210626_m1	NM_015873.3	74	Enterocyte
DPP4	Dipeptidyl-peptidase 4	1803	Hs00175210_m1	NM_001935.3	90	Enterocyte
SLC2A2	Facilitated Glucose Transporter 2 (GLUT 2)	6514	Hs01096908_m1	NM_000340.1	65	Enterocyte
GIP	Gastric Inhibitory Polypeptide	2695	Hs00175030_m1	NM_004123.2	78	Proximal
LCT	Lactase	3938	Hs00158722_m1	NM_002299.2	79	Enterocyte